Journal of Mechanics in Medicine and Biology
Vol. 17, No. 4 (2017) 1750037 (20 pages)

DOI: 10.1142/S0219519417500373

WALL SHEAR STRESS AND OSCILLATORY SHEAR INDEX DISTRIBUTION IN CAROTID ARTERY WITH VARYING DEGREE OF STENOSIS: A HEMODYNAMIC STUDY

PRASHANTH BASAVARAJA and ANISH SURENDRAN*

Department of Mechanical Engineering
National Institute of Technology Karnataka Surathkal
Mangalore 575025, Karnataka, India
**anish.surendran@gmail.com*

AJAY GUPTA

Department of Radiology
Weill Cornell Medical College
New York NY 10065, USA

LUCA SABA

Department of Radiology
Azienda Ospedaliero Universitaria (A.O.U.)
di Cagliari — Polo di Monserrato
S. S. 554 Monserrato, Cagliari 09045, Italy

JOHN R. LAIRD

UC Davis Vascular Center
University of California Sacramento
CA 95817, USA

ANDREW NICOLAIDES

Vascular Screening and Diagnostic Centre
London W1G 6LF, UK

Department of Biological Sciences
University of Cyprus, 1678 Nicosia, Cyprus

EDWARD E. MTUI and HEDIYEH BARADARAN

Department of Radiology
Weill Cornell Medical College
New York, NY 10065, USA

FRANCESCO LAVRA

Department of Radiology
Azienda Ospedaliero Universitaria (A.O.U.)
di Cagliari — Polo di Monserrato
S. S. 554 Monserrato, Cagliari 09045, Italy

JASJIT S. SURI

Point of Care Devices, Global Biomedical Technologies, Inc.
Roseville, CA 95661, USA

Diagnostic and Monitoring Division
AtheroPoint™ LLC, Roseville, CA 95661, USA

Electrical Engineering Department
Idaho State University, Pocatello, ID 83209, USA

Received 1 October 2015
Revised 10 February 2016
Accepted 4 May 2016
Published 27 July 2016

A significant proportion of cerebral stroke is a consequence of the arterial stenotic plaque rupture causing local thrombosis or distal embolization. The formation and subsequent rupture of the plaque depends on wall shear stress (WSS) and oscillatory shear index (OSI). The purpose of the present study was to understand the effect of hemodynamics on the spatial and temporal variations of WSS and OSI using realistic models with varying degree of carotid artery stenosis (DOS). Multiple CT volumes were obtained from subjects in the carotid bifurcation zone and the 3D models were generated. A finite volume-based computational fluid dynamics (CFD) method was utilized to understand the hemodynamics in pulsatile flow conditions. It was observed that high stenosis models occupied a large value of normalized WSS in the internal carotid artery (ICA) whereas they had smaller values of normalized WSS in the common carotid artery (CCA). For clinical use, the authors recommend using the spatial average value of oscillatory shear rather than the maximum value for an accurate knowledge about the severity of stenosis. The resultant vorticity changes the direction of spin after the bifurcation zone. Additionally, we propose the use of limiting streamlines as a novel and convenient method to identify the disturbed flow regions that are prone to atherogenesis.

Keywords: Stroke; carotid bifurcation; CT, wall shear stress; oscillatory shear stress.

1. Introduction

According to the statistics an estimated 6.7 million people died from stroke in 2012.[1] Among those who survive a stroke, a significant number suffer from severe disability given that stroke is a leading cause of serious long-term disability.[2] The most common type of stroke is the ischaemic stroke. Up to 15–20% of all strokes are secondary to atherosclerotic disease of the carotid arteries.[3] Progression of carotid artery atherosclerotic plaques can ultimately result in complete blockage of the carotid artery, though even lesser degrees of carotid vessel narrowing (stenosis) can increase the risk of stroke in patients. The atherosclerotic plaque in the carotid arteries most commonly forms near the bifurcation zone and curved regions of the vessel. These locations are vulnerable to high flow disturbances leading to low wall shear stress (WSS)[4–7] suggesting that blood fluid dynamics (hemodynamics) has an

*Corresponding author.

important role in deciding the formation and development of the atherosclerotic plaques.

The objective of the present study was to understand the effect of hemodynamics on the spatial and temporal variations of WSS and oscillatory shear index (OSI) using realistic models with varying degree of stenosis (DOS). We aimed to establish a connection between the bulk flow hemodynamics with the wall shear and oscillatory shear stress. Additionally, we propose the use of limiting streamlines as a novel and convenient method to identify the disturbed flow regions that are prone to atherogenesis.

The correlations of low WSS and oscillating shear stress with the intima thickening and atherosclerosis progression are described in several studies.[4,8–12] The magnitude of WSS at the bifurcation zone and in the internal carotid artery (ICA) greatly depends on the upstream flow conditions in the common carotid artery (CCA). This includes mainly the patient-specific velocity waveform[13,14] and the turbulent intensity.[15] The other parameter that significantly influences the wall shear is the morphology of the vessel lumen. A subtle change in the geometry, caused by atherogenesis, can affect the fluid dynamics greatly.[16–18] The extent of blockage due to atherosclerotic lesions in the ICA is quantified in terms of the DOS.[19] In order to understand the localization of atherogenesis, numerical simulations in realistic patient-specific geometries are very essential. The use of computational fluid dynamics (CFD) results for clinical usage is still not fully matured due to the lack of standardization and proper validation.[20,21] Much of the earlier fluid dynamical studies on the blood flow have been done on idealized models.[12–14,18,22,23] Though a good number of studies is there *in vivo* condition, they have been done under the assumptions of laminar flow and/or Newtonian fluid.[18,23–25] An accurate assessment of WSS and its connection to the bulk flow hemodynamics is essential for studies on the pathogenesis of atherosclerosis.

In the present investigation, computational simulation was carried out to understand the effect of DOS on the temporal and spatial variations of wall shear and oscillatory shear on realistic geometries. The study was undertaken on four different subjects whose DOSs are 41%, 56%, 62% and 69%. The authors proposed the use of limiting streamlines as a novel and convenient method to identify the probable locations of the plaque progression. The current numerical scheme has been properly validated with the previous studies.

2. Methods

The patients in the current study are a subset of the sample of patients studied in previous works by this group[26,27] focused on correlation of plaque imaging characteristics and symptomatic disease. This study, including the retrospective review of clinical standard of care imaging data performed between August 2009 and March 2014, was approved by the Human Subjects Institutional Review Board of our institution. Of note, the DICOM imaging data analyzed for this study contains no

protected health information. Moderate-to-high-grade extra-cranial ICA stenosis (50–99% stenosis) was measured using CT angiography studies. The detailed method for NASCET stenosis measurement is described in these prior works,[26,27] though of note the DOS used for our analysis was not based on NASCET-style measurements (see below). The presence of significant detectable calcium in the atherosclerotic plaque was ascertained qualitatively and subjectively. Atherosclerotic plaques included in this study were analyzed by a board-certified neuro-radiologist to determine the single axial source image with greatest luminal diameter narrowing.

2.1. *Geometry reconstruction and meshing*

A series of scanned Computed Tomography (CT) images of four patients covering the carotid bifurcation artery with significant carotid artery stenosis, lumen and wall surface of the carotid bifurcation was obtained. The DOSs of all the patients were calculated based on the relative minimum diameter ($D_{\min}$) of the ICA with respect to the diameter of the non-stenosis region (D) in the CCA.

$$\text{DOS} = \left(1 - \frac{D_{\min}}{D}\right) \times 100\%. \tag{1}$$

Table 1 shows the DOS for each patient selected for the present investigation. Of note, we did not perform NASCET-type stenosis measurements which require the use of the distal ICA diameter as a denominator for stenosis measurements.[28] A series of scanned images is shown in Fig. 1(a), for a representative model, to demarcate the CCA, ICA, external carotid artery (ECA) and the bifurcation regions. The bright white spot in the image represents the calcium deposit within the plaque. The lumen portion was traced out from the CT image using an in-house software (ImgTracer^{TM}, courtesy of AtheroPoint, Roseville, CA, USA). The output of the ImgTracer^{TM} is the xy-coordinates in terms of pixels. This was further converted into mm (based on the resolution) and then fed into a commercially available 3D geometry modeler ICEM CFD to prepare the required polylines (Fig. 1(b)) upon which the surface will be created (Fig. 1(c)). Smoothening of the surface was done using another 3D modeling software CATIA. The 3D computational models of the four geometries are shown in Fig. 2. For the present study the computational simulations are carried out using a finite volume method (FVM). Unstructured

Table 1. DOS calculated for each patient.

Patient no.	DOS (%)
Patient 1	62
Patient 2	41
Patient 3	56
Patient 4	69

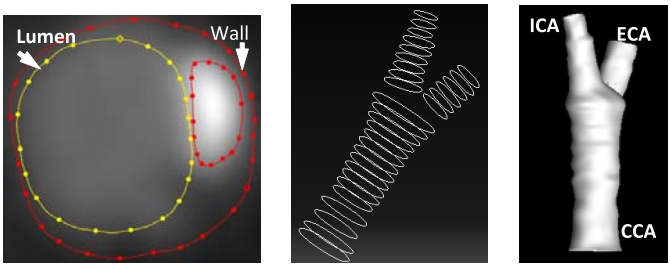

(a) (b) (c)

Fig. 1. (a) Tracing of the vessel lumen with image tracer. (b) Traced points are converted into polylines in ICEM CFD. (c) Final 3D model generated using CATIA.

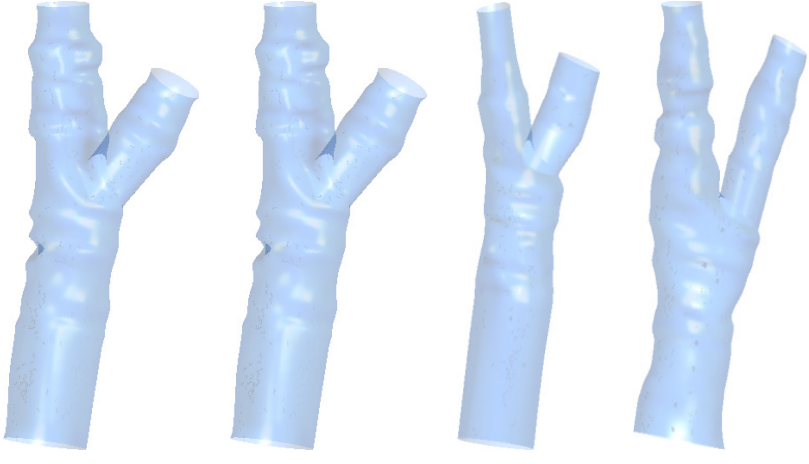

(a) *Patient* 1. (b) *Patient* 2. (c) *Patient* 3. (d) *Patient* 4.

Fig. 2. Carotid bifurcation models for the four models, showing the CCA, ECA and ICA.

tetrahedral elements are used for grid generation. Prism elements are attached to the walls in order to capture the boundary layer effects.

2.2. *Fluid models and boundary conditions*

Blood was modeled as an incompressible, homogeneous viscous fluid, with a density of 1060 kg/m^3. The rheological model of blood has been studied by several researchers[10,29,30]; accordingly, it is treated as non-Newtonian using the Carreau–Yasuda model. The numerical simulations are carried out using a well-established solver, CFX 14.0. The governing equations are the time-dependent Navier–Stokes equations.[10]

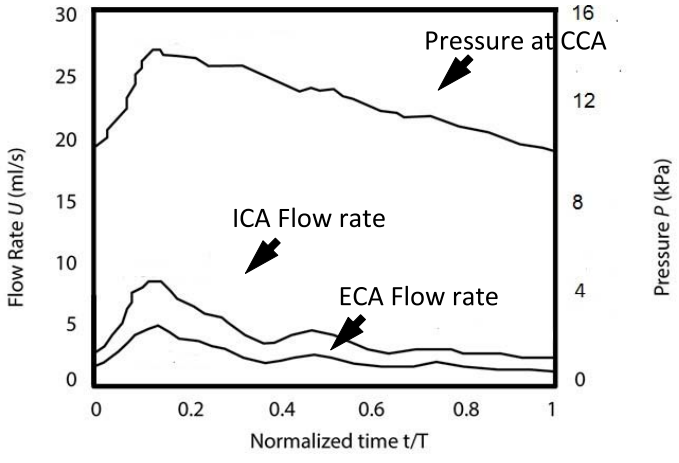

Fig. 3. Inlet pressure as a function of normalized time used for the simulation within the carotid bifurcation. The corresponding flow rates at the exits of ICA and ECA are also shown.

For flows with pressure-induced separation, the shear stress transport (SST) model would provide more realistic answers.[31] Hence, for the present study SST model is employed for solving the turbulent parameters. A time varying pressure boundary condition is specified at the inlets and a time varying velocity profile is set at the ends of ICA and ECA (Fig. 3). The specified values are spatially uniform, but pulsating with respect to time. The assumed pulse frequency is 80 strokes per min. Time-dependent behavior for unsteady simulations is specified through time period and time step. A time step (t) of 0.001 s is specified and the iterations are carried out till the convergence criteria is met.

As the patient-specific boundary conditions were not available for each individual patient, similar flow waveform is assumed for all the cases. In order to avoid

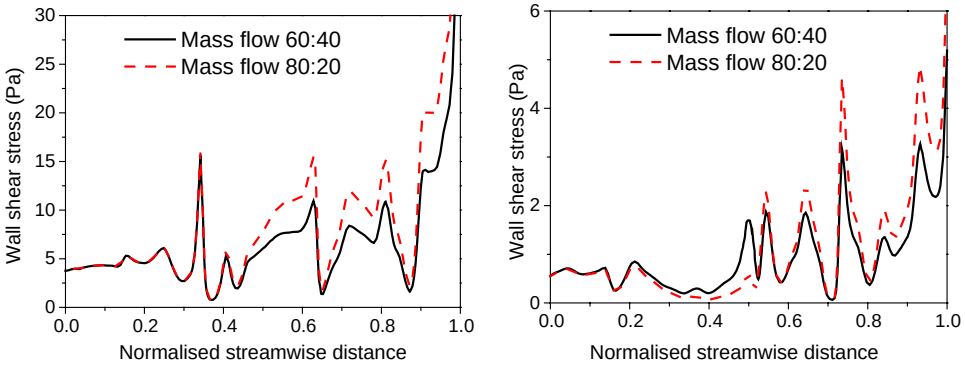

(a) (b)

Fig. 4. Variations of WSS on the outer wall of the lumen vessel at deceleration time step (0.45 s) for (a) *patient* 2 and (b) *patient* 4.

the discrepancies in the results, due to this assumption, the results are normalized with respect to their corresponding average while comparison. An additional advantage of assuming similar flow waveform at the inlets of all the domains is that it would separate out the effect of lumen geometry while comparing the flow patterns in these domains. The effect of variation in the boundary condition has been studied by varying the mass flow rates through the ICA and CCA. Figure 4 shows the WSS variations for two patients for two different mass flow rates. In the first case, the ratio of percentage mass flow rates through ICA and ECA is 60:40 and in the second case it is 80:20. It can be observed that the WSS pattern on the lumen surface is exactly similar, qualitatively. As the mass flow rates through the ICA increase the WSS has to increase proportionally and this is visible from these plots. This proves that whatever be the mass flow ratio through ICA and ECA, for a given lumen geometry the wall shear patterns on the wall will be similar.

3. Results

3.1. *Effect of DOS on WSS and OSI*

The WSS in the vessel lumen is a function of the inlet velocity at the CCA. As the inlet velocities for all these models were different, this variation will reflect in the WSS comparison also. In order to avoid this, WSS values were normalized with their corresponding average values and then the comparison was made with different models. The temporal and spatial variations of WSS at the inner as well as outer walls of ICA were noted down. Two polylines were created; the outer one running from the CCA inlet to the ICA outlet and the inner one running from the bifurcation zone to ICA outlet (Fig. 5(a)) at systolic peak and the spatial average of

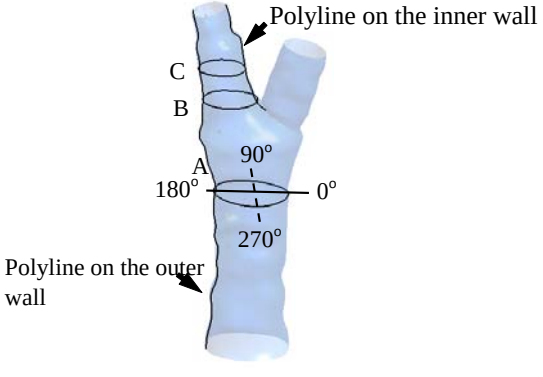

(a)

Fig. 5. (a) Representative model showing specific locations where the WSS values are extracted. Variations of the normalized WSS during peak systole (b) on the outer wall of the vessel lumen, (c) on the inner wall, (d) on a point at the outer wall during pulsatile flow and (e) on a point at the inner wall during pulsatile flow.

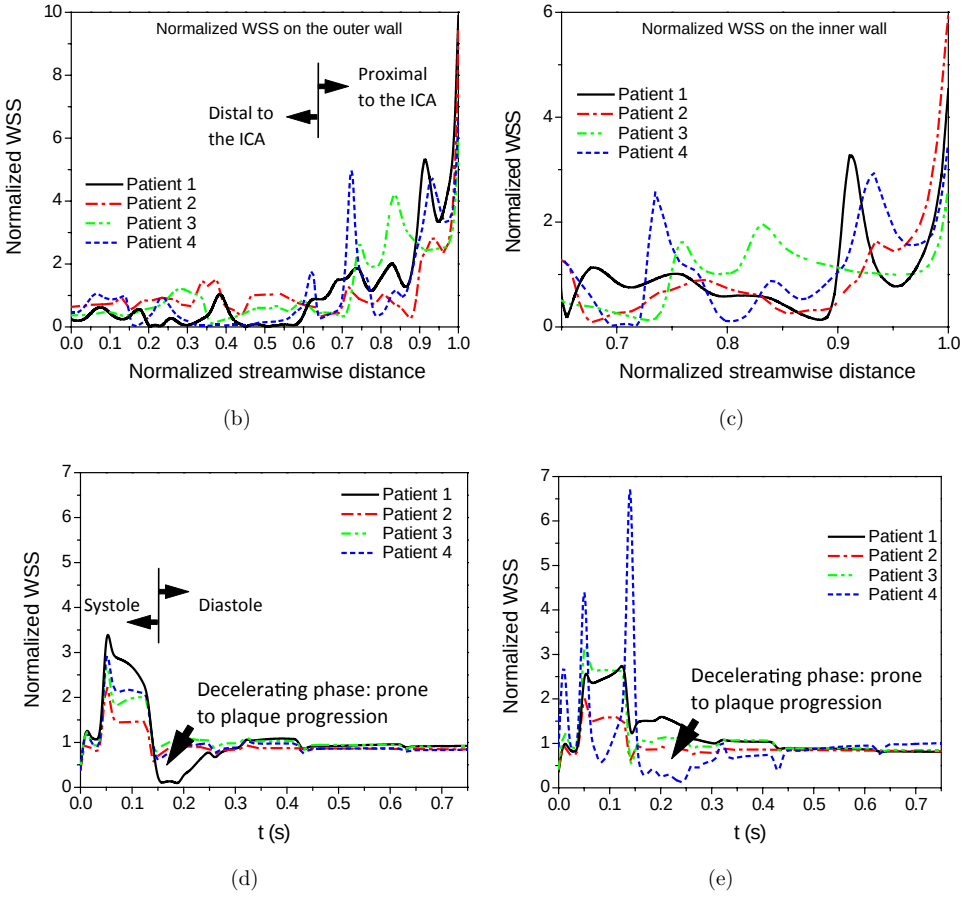

Fig. 5. (*Continued*)

WSS along the respective line was used for the normalization. Figures 5(b)–5(c) show the variations of the normalized WSS along the inner and outer walls of the vessel lumen.

The variations of WSS on the outer walls of the four models revealed that up to the bifurcation zone WSS was maximum for *patient* 2 (low DOS model), and it was minimum for the *patient* 1 (high DOS model). Note that the bifurcation zone starts at a normalized distance of around 0.64. After the bifurcation zone, the normalized WSS value suddenly increased for *patient* 1 due to the protrusion of the plaque, which restricted the effective flow area.

These characteristics indicate that with high stenosis, models occupy a large value of normalized WSS in the ICA whereas they have smaller values of normalized WSS in the CCA. The peak-to-trough variations were lower for *patient* 2, which was attributed to the patient's lower value of DOS. Just after the bifurcation zone a sudden rise was observed for *patient* 4, followed by a sharp trough also. This

low normalized WSS region may be identified as a hotspot for further plaque progression. The peaks in the graph correspond to the protruded plaques into the vessel lumen. The fluid accelerates here creating a high WSS. Each protrusion is followed by a low velocity wake region causing potential zone for the progression of atherosclerotic plaques.

The temporal variation of normalized WSS was noted at two points on either side of the location B. The peak value of WSS occurs during systole, and the least value occurs at the decelerating phase of the systole (Figs. 5(d) and 5(e)), indicating that the decelerating phase is the most conducive phase for atherogenesis. At the outer wall, *patient* 1 showed large temporal variations in the WSS value, while at the inner wall they were shown by the *patient* 4. Hence, for *patient* 4 further chances of atherosclerosis progression occur at the inner wall of the ICA.

Figures 6(a)–6(d) show the angular variations of the normalized WSS along the circumference at three different axial locations, A, B and C (Fig. 5(a)). The normalized WSS values were plotted at peak systole at different theta values with the radius showing the magnitude of the normalized WSS. The circumferential non-uniformity of the shear stress is quite visible from these plots. As the flow proceeds through the ICA, the peak value of shear stress shifts from one angular location to another due to the secondary flows. The locations where the WSS value becomes zero are recirculation/separation zones. Such a disturbed flow region occurs at 270° for *patient* 4 in the CCA.

OSI measures the cyclic departure of the WSS vector from its predominant flow direction. A high value of OSI indicates a severe compression and stretching of the lumen wall which accelerates the plaque rupture. It is defined as

$$\mathrm{OSI} = \frac{1}{2}\left(1 - \frac{\left|\int_0^n \tau\right|}{\int_0^n |\tau|}\right). \tag{2}$$

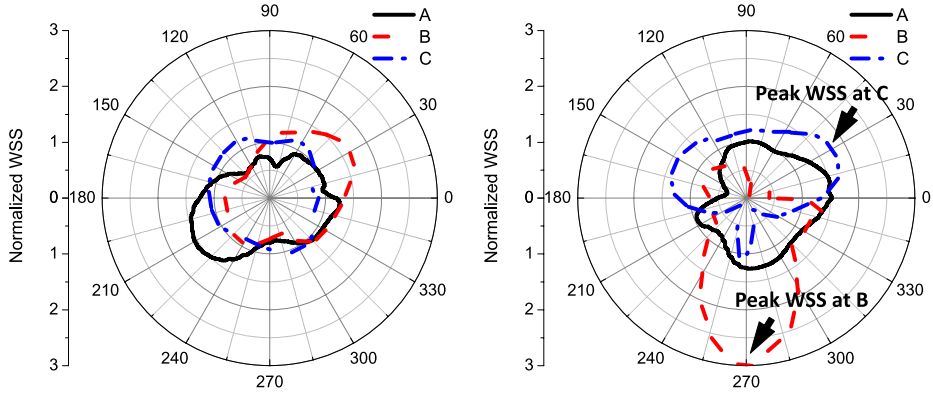

Fig. 6. Angular variations of normalized WSS at different axial locations for (a) *patient* 1, (b) *patient* 2, (c) *patient* 3 and (d) *patient* 4.

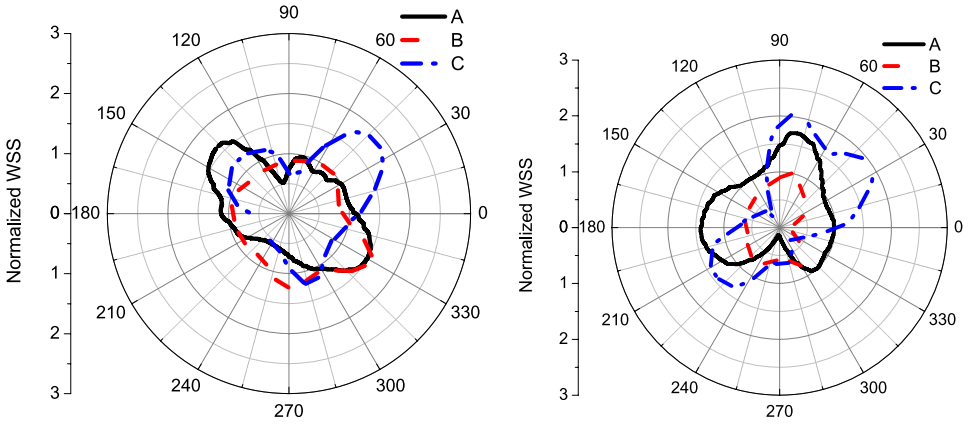

Fig. 6. (*Continued*)

The variations of OSI along the inner and outer walls of ICA are shown in Figs. 7(a) and 7(b). The magnitudes of the oscillatory shear are high for *patient* 1 and *patient* 4 and they are spread over a wider region along the circumference of the wall compared to *patient* 2 and *patient* 3. The angular variations of OSI indicate a high level of risk for *patient* 1 and *patient* 4 (Figs. 7(c)–7(f)). The larger magnitude of oscillatory shear implies a higher stretching and compression of the vessel wall which can cause sufficient damage to the endothelial cells. Higher OSI values along the circumference imply higher risk for plaque rupture in that region. The location of the maximum OSI may not be correlating with the location of the peak shear stress. On the contrary, the OSI values are high where the flow disturbances are more.

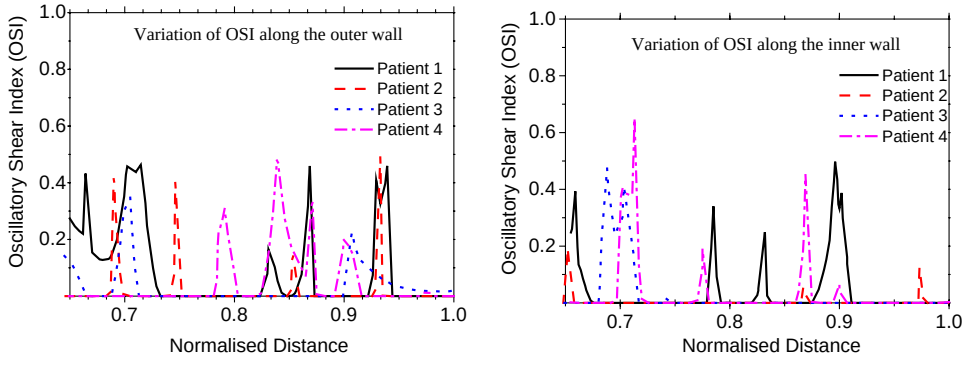

Fig. 7. Variations of OSI (a) on the outer wall of the vessel lumen and (b) on the inner wall Angular variations of OSI at different axial levels for (c) *patient* 1, (d) *patient* 2, (e) *patient* 3 and (f) *patient* 4 (the angular arrows show the circumferential regions where the OSI value is zero).

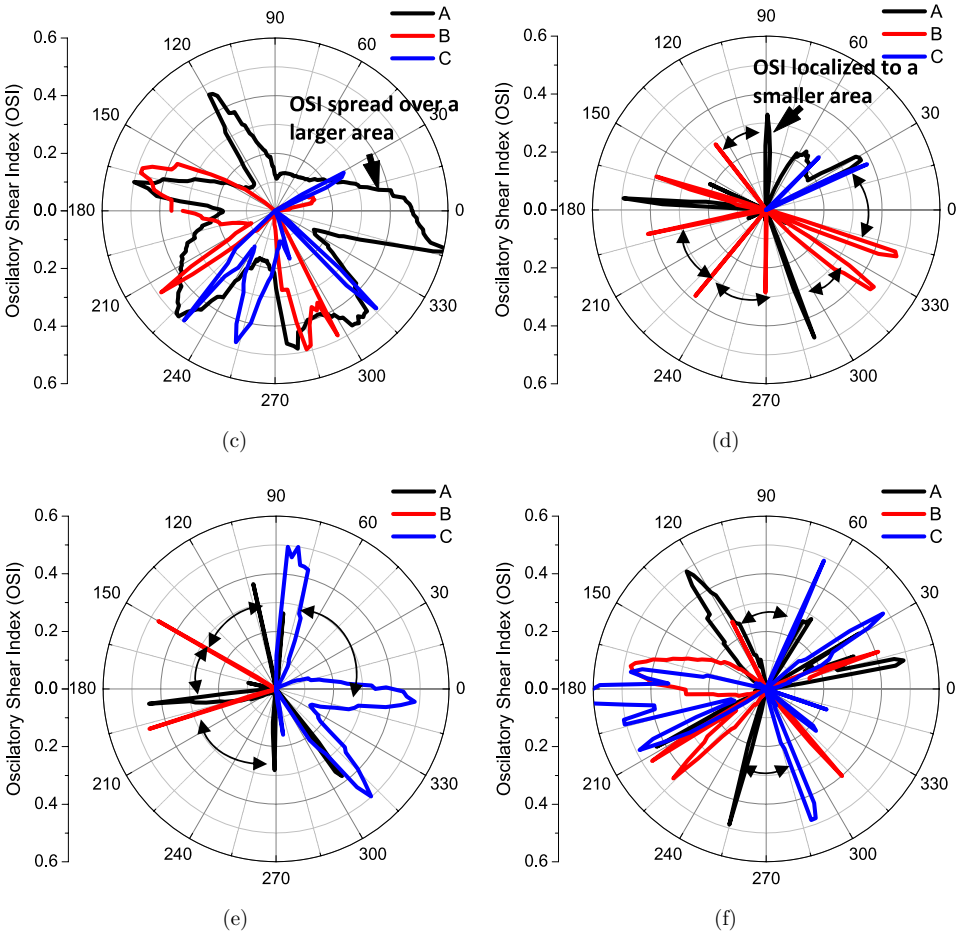

Fig. 7. (*Continued*)

In the ICA region, maximum oscillatory shear is observed for *patient* 4 and the minimum is observed for *patient* 2. For *patient* 2, high level of oscillatory shear can be observed at certain localized points inside the ICA. The angular arrows in Fig. 7 represent the circumferential regions where the OSI value is zero. For *patient* 2 and *patient* 3, the OSI values are almost nil around the periphery of the vessel lumen, which implies they are at less risk. With higher DOS the flow becomes more rotational in the vicinity of plaques causing the oscillatory shear to have high non-zero values at these locations.

3.2. *Understanding the bulk flow behavior through limiting streamlines plots*

In this subsection, a novel way is described to identify the disturbed flow regions in carotid artery bifurcation. Observing the behavior of surface streamlines, otherwise

known as limiting streamlines, helps to understand the secondary flows, region of separation and reattachement points. The magnitude of WSS depends on the velocity vectors near the surface. In Fig. 8(a), surface streamlines during peak systole are shown. The patterns of the surface streamlines are different in each case and they solely depend on the irregularity of the vessel lumen. Just before the bifurcation zone a line of separtion can be observed for all the cases.

In the regions where the plaqe thickness is high, the intima region projects deep into the lumen and the streamlines flow around to form a low velocity wake region at the downstream. This further reduces the WSS at the downstream, which enhances

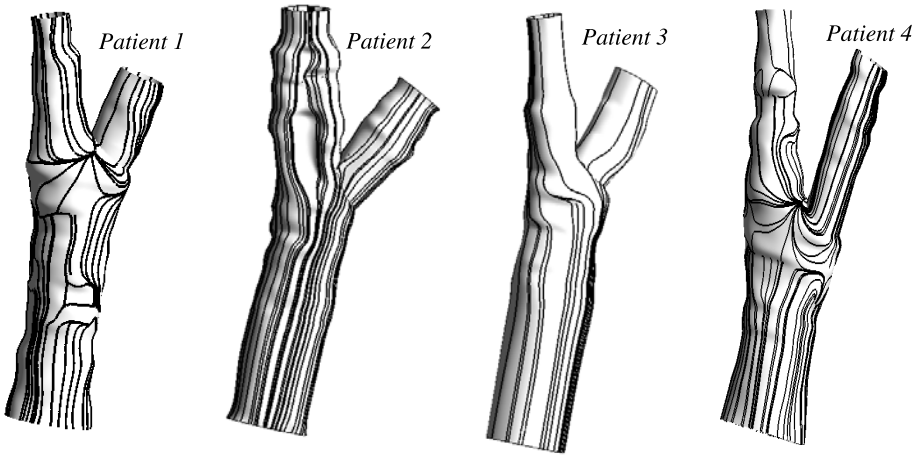

(a)

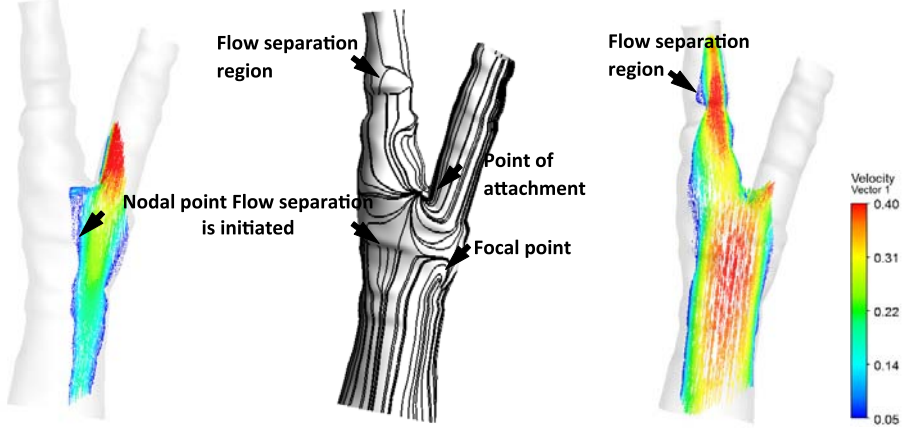

(b)

Fig. 8. (a) Surface streamlines during peak systole ($t = 0.1$ s) for different geometric models. (b) Limiting streamlines are shown along with the flow vectors inside the flow passage for *patient* 4.

the deposition. Secondary flow originates in the bifurcation region and spirals through the ICA. The stenosis in the ICA region is asymmetric which results in non-uniform velocity contours. It can be seen that for *patient* 2 the streamlines are almost straight and devoid of any secondary flow patterns. However, this is not the case with *patient* 1 and *patient* 4, where large cross-flows are observed.

The behavior of the fluid flow can be understood by the nodal points and focal points. The nodal point of attachment can be identified from the lines that emerge from the point and spread out over the surface. On the other hand, the nodal point of separation acts as a sink where the lines may vanish.[32] A focus is formed when a number of limiting streamlines spiral around the singular point, either away from it (a focus of attachment) or into it (a focus of separation) and it generally occurs in the presence of rotation. The analysis of limiting streamlines for one representative model (*patient* 4) is shown in Fig. 8(b). For better understanding, flow vectors are plotted on two longitudinal planes and are shown here. Corresponding to the nodal points, flow separation regions are visible from the flow vectors. In a similar fashion with the help of limiting streamlines, flow separation regions can be identified along the flow passage. A point of attachment is seen at the bifurcation zone where the limiting streamlines are going outwards. In the CCA, a focal point is visible indicating the presence of swirl.

3.3. *Resultant vorticity contours*

The swirling strength of the flow can be measured by calculating the resultant vorticity. In the present analysis it is observed that the vorticities in the X- and Y-directions are prominent compared to that in the Z-direction. The Z-direction is aligned with the normal to the inlet of the CCA. Figure 9(a) shows the direction of

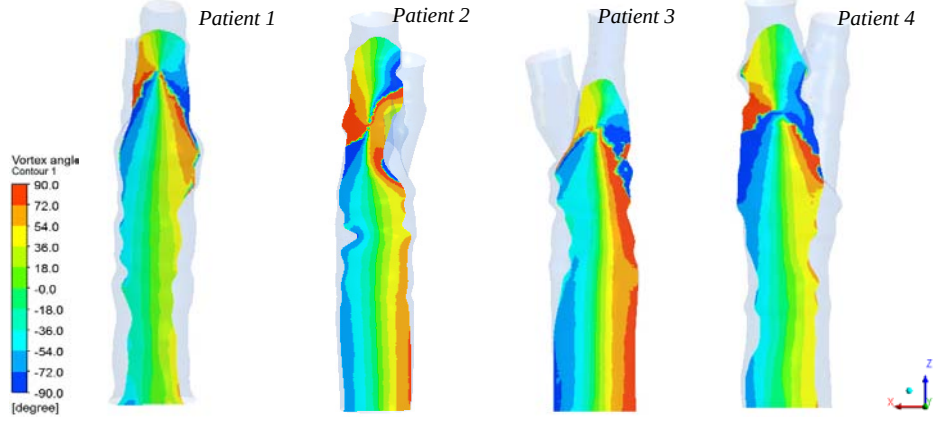

(a)

Fig. 9. (a) The resultant vorticity angles with respect to X-axis. (b) The resultant vorticity angles at three different longitudinal planes for *patient* 1 (arrow indicates location of spin change).

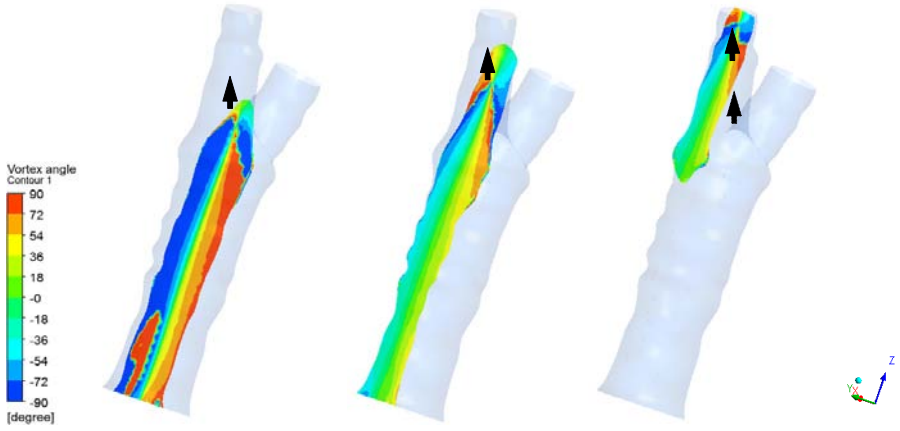

(b)

Fig. 9. (*Continued*)

the resultant vorticity with respect to X-axis on the ZX-plane. From the positive Y-direction, a counterclockwise rotation is indicated by the red color and a clockwise rotation is shown with blue. The change in the vorticity angle reveals that after bifurcation zone a change of spin happens with the resultant vorticity. This change of spin is caused by the secondary flows that originated from the inner wall of the bifurcation zone to the outer wall. It is to be noted that the location at which this direction change happens moves toward from the inner wall of ICA to the outer wall. This can be seen in Fig. 9(b) where the vorticity angles are is plotted in three different planes for *patient* 1. This phenomena is observed in the other models as well. The resultant vorticity direction changes not only at the bifurcation zone, but it changes wherever the secondary flows are significant.

4. Verification and Validation

Verification and validation are two important steps in any CFD simulations. The verification process examines the accuracy in the models through comparison to exact analytical results. Roache[33] identified that grid-convergence studies are the most reliable technique for the quantification of numerical uncertainty. The results of such a study are shown for one representative model (*patient* 1) in Fig. 10. For *patient* 1, grid with 411,453 elements was selected for further simulations, considering that the difference in the velocity profile in comparison with fine grids (610,308) is negligible.

The present computational methodology is validated with the established results of Perktold *et al.*[10] The WSS at the internal wall of ICA is plotted at two different locations; one at the bifurcation zone and the second just after the stenosis region in ICA. Figure 11 shows the results obtained from the present simulation compared with the results obtained by Perktold *et al.* The WSS plots are in good agreement at

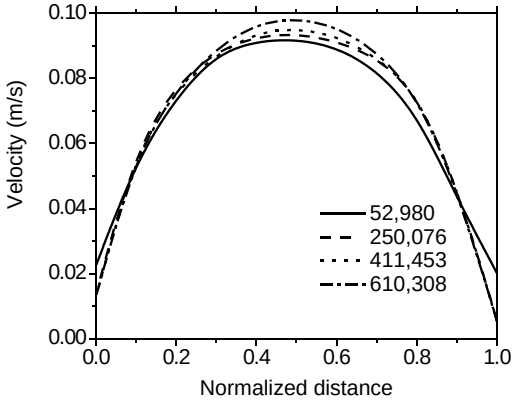

Fig. 10. Velocity profiles inside the CCA of *patient* 1 for various numbers of grid elements.

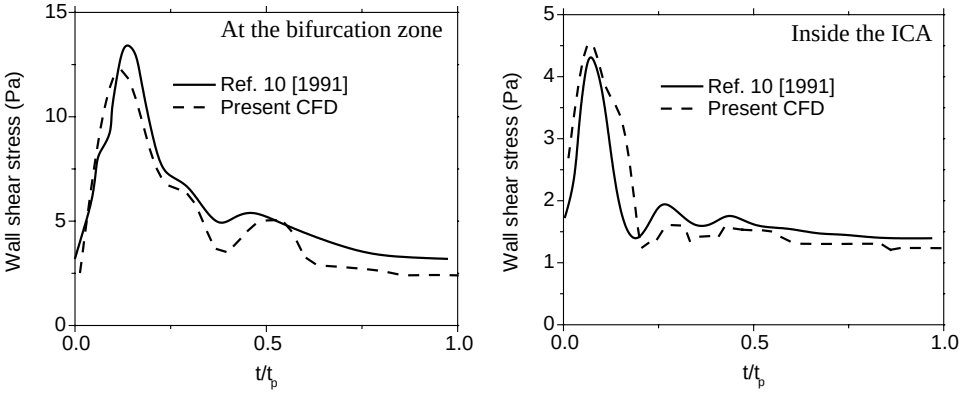

Fig. 11. The WSS variations during the pulsatile cycle at the internal walls of ICA at bifurcation zone and after the bifurcation zone (inside ICA).

these locations. There is a slight underprediction for the peak WSS at the bifurcation zone. However, the plots are coinciding during most of the pulsatile time steps. These plots prove that the current CFD methodology is quite accurate to predict the hemodynamics in the carotid bifurcation.

5. Discussions

In the present investigation, an attempt was made to understand the effect of DOS on atherosclerotic plaque development and the bulk flow hemodynamics using realistic models. The proposed novel way of limiting streamlines in showing the separated flow regions, in other words the probable atherogenesis zones, is an easy and simple way that connects the atherogenesis to the bulk flow hemodynamics.

This study explores the effect of DOS on the temporal and spatial variations of wall shear and oscillatory shear. Variations in the oscillatory shear contribute to the enhancement of atherosclerosis in the arterial system.[14] The magnitudes of the oscillatory shear are high for *patient* 1 and *patient* 4 and they are spread over a wider region along the circumference of the wall. For the low DOS models (*patient* 2 and *patient* 3), the oscillatory shear is absent at a majority of regions, instead it appears only at certain localized regions. While the maximum values of OSI are comparable with different DOS models, their average value throws a different picture. Hence, for clinical use, in order to represent the severity, it is recommended to use the average value of oscillatory shear than the maximum value. It is observed that the high DOS models (DOS above 60%) occupy a smaller values of normalized WSS in the CCA, but after the bifurcation zone the spatial and transient average shear stress rises with DOS. While comparing models with different DOSs it is recommended to compare the normalized value of shear stress rather than its absolute value in order to understand the severity of atherogenesis progression.

The bulk flow fluid dynamics in the carotid bifurcation zone is analyzed in terms of the resultant vorticity direction. The analysis revealed that after the bifurcation zone a change of spin happens with the resultant vorticity and the location at which this direction change happens moves toward from the inner wall of ICA to the outer wall. The variation of angular location of the peak shear stress inside the ICA is in correlation with this bulk flow hemodynamics.

Table 2 shows the comparison of some of the critical attributes between the four models. Turbulence has a major role in the thrombogenesis and the mass transfer between the endothelial cells and the blood. Sarah and Poepping[34] detected a transitional flow in 50–70% of stenotic models through their study, *in vitro*, wherein the surface undulations are not taken into account. In the present analysis, it was observed that for a high stenosis of 66% (*patient* 4) the turbulent intensity is 8% at the stenotic region (Table 2). This is a local maximum and within the computational model this may be even higher. However, for *patient* 2 the turbulent intensity is only 0.1%, which means a laminar modeling may be sufficient with a low DOS. These results are in accordance with the studies conducted by May *et al.*,[35] in rat carotid artery. It could appear that a threshold DOS value of 60% generates a turbulent intensity more than 5%. However, this may not be seen as a general result as the

Table 2. Comparison of few critical attributes between the various computational models.

Attributes compared	*Patient* 1	*Patient* 2	*Patient* 3	*Patient* 4
DOS (%)	61.5	41.0	56.2	69.1
Turbulent intensity (%)	6.6	0.1	0.85	8
OSI average outer wall	0.22	0.016	0.056	0.10
OSI maximum (outer wall)	0.60	0.48	0.50	0.5
OSI average (inner wall)	0.05	0.02	0.04	0.08
OSI maximum (inner wall)	0.50	0.48	0.57	0.65

present study has been done only on four models. Even though the maximum values of OSI are comparable for different DOS models, the average oscillatory shear stress of *patient* 4 (DOS = 69%) is 300% higher than that of *patient* 2 (DOS = 41%) at the outer wall and it is 400% higher at the inner wall.

WSS is a key factor in determining the morphology, orientation and permeability of the endothelial cells.[36,37] WSS is primarily derived from the velocity gradient near the wall. The importance of geometry in deciding the hemodynamics patterns is brought out by many computational researches in the last decade.[18,25,38] Marked difference in the secondary flow pattern is observed between the idealized and realistic models.[25] Another factor which may not be captured in an *in vitro*/idealized model analysis is the asymmetric nature of the stenosis. An asymmetric stenosis predicts a higher shear stress and larger separation compared to a symmetric one.[18] Though the effect of DOS on hemodynamics is studied only by quite a few researchers, most of them were on idealized/*in vitro* models.[13,14,22,34] An *in vivo* computational study by Gallo *et al.*[38] provided a relationship between helicity-based bulk flow descriptors and disturbed shear indicators using a Newtonian flow assumption. A comparison has been made between the present work and some of the major previous works and it is brought out that most of the numerical studies in the carotid bifurcation did not consider the effect of turbulence and they modeled it as a laminar flow (Table 3). However, from the values of turbulent intensity (Table 2), it has been proven that for higher DOS cases the numerical modeling has to be turbulent. The present study has been done on realistic models generated through the CT scan images of the carotid artery. The non-Newtonian nature as well as the turbulent nature of the fluid have been considered, which were not considered by most of the other researchers.

The study has the following limitations. The lumen wall is assumed as a rigid wall, neglecting the real elastic nature. More accurate analysis can be made by carrying out the fluid structure interaction of these models. Another assumption involved in the present simulation is regarding the boundary condition. The present

Table 3. Comparison of the present work with some of the major previous works based on varying DOSs in carotid artery.

Reference	% Stenosis	Model	Newtonian/ non-Newtonian	Laminar/ transitional/turbulent	Grid dependency study
Ref. 4	—	*In vitro*	Newtonian	—	—
Ref. 25	—	*In vivo*	Newtonian	Laminar	—
Ref. 18	70%	Ideal	Newtonian	Laminar	—
Ref. 22	75%	Ideal	Newtonian	—	Yes
Ref. 24	—	*In vivo*	Newtonian	—	—
Ref. 14	70%	Ideal	Newtonian	Laminar	Yes
Ref. 38	—	*In vivo*	Newtonian	Laminar	—
Ref. 34	50% and 70%	*In vitro*	Non-Newtonian	Transitional	—
Present study	41–46%, 61% and 69%	Realistic	Non-Newtonian	Turbulent	Yes

boundary conditions are taken from the literature and similar boundary conditions are applied for all the four models irrespective of their DOSs.

6. Conclusions

Computational simulation of four realistic models is carried out to understand the effect of DOS on the temporal and spatial variations of wall shear and oscillatory shear. The authors recommend the use of normalized WSS rather than the actual wall shear while comparing cases with varying stenosis. The high DOS models show smaller values of normalized WSS in the CCA but a larger value in the ICA. For clinical use, in order to represent the risk, it is recommended to use the average value of oscillatory shear than the maximum value. The authors propose the use of limiting streamlines as a novel and convenient method to identify the probable locations of the plaque progression. The bulk flow hemodynamics is represented with the direction of resultant vorticity. It reveals that after the bifurcation zone a change of spin happens with the resultant vorticity due to the secondary flows that originated from the inner wall of the bifurcation zone. The above conclusions are made from the study on four realistic models without considering the elastic nature of the lumen wall.

References

1. WHO, Cardiovascular Diseases Fact Sheet No. 317 (updated March 2013), WHO Fact Sheets 2013.
2. Mozzafarian D *et al.*, Heart disease and stroke statistics — 2015 update: A report from the American Heart Association, *Circulation* **131**:e29–e322, 2015.
3. Grotta JC, Clinical practice: Carotid stenosis, *N Engl J Med* **369**:1143–1150, 2013.
4. Ku DN, Giddens DP, Zarins CK, Glagov S, Pulsatile flow and atherosclerosis in the human carotid bifurcation: Positive correlation between plaque location and low oscillating shear stress, *Arteriosclerosis* **5**:293–302, 1985.
5. Malek AM, Alper SL, Izumo S, Hemodynamic shear stress and its role in atherosclerosis, *JAMA* **282**:2035–2042, 1999.
6. Canchi T, Kumar SD, Ng EYK, Narayanan S, A review of computational methods to predict the risk of rupture of abdominal aortic aneurysms, *Biomed Res Int* **2015**:861627, 2015.
7. Ng EYK, Siauw WL, Modelling of fluid-wall interactions for viscous flow in a stenotic elastic artery, *Prog Comput Fluid Dyn* **2**(1), 33–44, 2002.
8. Friedman MH, Bargeson CB, Deters OJ, Hutchins GM, Mark FF, Correlation between wall shear and intimal thickness at a coronary artery branch, *Atherosclerosis* **68**:27–33, 1987.
9. Giddens DP, Zarins CK, Glagov S, The role of fluid mechanics in the localisation and detection of atherosclerosis, *J Biomech Eng* **115**:588–594, 1993.
10. Perktold K, Resch M, Peter RO, Three-dimensional numerical analysis of pulsatile flow and wall shear stress in the carotid artery bifurcation, *J Biomech* **24**:409–420, 1991.
11. Soudah E, Ng EYK, Loong TH, Bordone M, Pua U, Narayanan S, CFD modelling of abdominal aortic aneurysm on hemodynamic loads using a realistic geometry with CT, *Comput Math Methods Med* **2013**:472564, 2013.

12. Ng EYK, Siauw WL, Chong CK, Simulation of oscillatory wall shear stress in channels with moving indentations, *Int J Numer Methods Eng* **54**(10):1477–1500, 2002.
13. Antonova N, Xu D, Velcheva I, Kaliviotis E, Tosheva P, Stenosis effects on the fluid mechanics of the common carotid artery bifurcation for unsteady flows, *J Mech Med Biol* **15**:1540008, 2015.
14. Li ZY, Gillard JH, Tavian V, Tang T, Sadat U, Young V, Patterson A, Graves M, The mechanical triggers of plaque rupture: Shear stress vs pressure gradient, *Br J Radiol* **82**:39–45, 2009.
15. Tan F *et al.*, CFD study on flow disturbance in a stenosed carotid artery bifurcation, *J Biomech* **41** (S1):S477, 2008.
16. Karino T, Motomiyza M, Flow visualisation in isolated transparent natural blood vessel, *Biorheology* **20**:119–127, 1983.
17. Perktold K, Resch M, Numerical flow studies in human carotid artery bifurcations: Basic discussion of the geometric factor in atherogenesis, *J Biomech Eng* **12**:2111–2123, 1990.
18. Tang D, Yang C, Kobayashi S, Zheng J, Vito RP, Effect of stenosis asymmetry on blood flow and artery compression: A three-dimensional fluid-structure interaction model, *Ann Biomed Eng* **31**:1182–1193, 2003.
19. Casscells W, Naghavi M, Vulnerable atherosclerotic plaque: A multifocal disease, *Circulation* **107**:2072–2075, 2003.
20. Steinman DA, Computational modelling and flow diverters: A teaching moment, *AJNR Am J Neuroradiol* **32**:981–983, 2011.
21. Taylor CA, Steinman DA, Image-based modelling of blood flow and vessel wall dynamics: Applications, methods and future directions, *Ann Biomed Eng* **38**:1188–1203, 2010.
22. Prosi M, Perktold K, Schima H, Effect of continuous arterial blood flow in patients with rotary cardiac assist device on the washout of a stenosis wake in the carotid bifurcation: A computer simulation study, *J Biomech* **40**:2236–2243, 2007.
23. Siauw WL, Ng EYK, Mazumdar J, Unsteady stenosis flow prediction: A comparative study of non-Newtonian models with operator splitting scheme, *Med Eng Phys*, **22**(4):265–277, 2000.
24. Maurits NM, Loots GE, Veldman AE, The influence of vessel wall elasticity and peripheral resistance on the carotid artery flow wave form: A CFD model compared to *in vivo* ultrasound measurements, *J Biomech* **40**:427–436, 2007.
25. Zhao SZ *et al.*, Blood flow and vessel mechanics in a physiologically realistic model of a human carotid arterial bifurcation, *J Biomech* **33**:975–984, 2000.
26. Gupta A *et al.*, Evaluation of computed tomography angiography plaque thickness measurements in high-grade carotid artery stenosis, *Stroke* **45**:740–745, 2014.
27. Gupta A *et al.*, CT angiographic features of symptom-producing plaque in moderate-grade carotid artery stenosis, *AJNR Am J Neuroradiol* **36**:349–354, 2015.
28. Fox AJ, How to measure carotid stenosis, *Radiology* **186**:316–318, 1993.
29. Lee SW, Steinman DA, On the relative importance of rheology for image based CFD models of the carotid bifurcation, *J Biomech Eng* **129**:273–278, 2007.
30. Morbiducci U *et al.*, On the importance of blood rheology for bulk flow in hemodynamic models of the carotid bifurcation, *J Biomech* **44**:2427–2438, 2011.
31. Menter FR, Two-equation Eddy-viscosity turbulence models for engineering applications, *AIAA J* **32**:1598–1605, 1994.
32. Tobak M, Peake DJ, Topology of three-dimensional separated flows, *Annu Rev Fluid Mech* **14**:61–85, 1982.
33. Roache PJ, *Verification and Validation in Computational Science and Engineering*, Hermosa Publishers, New Mexico, 1998.

34. Sarah K, Poepping TL, Transitional flow analysis in the carotid artery bifurcation by proper orthogonal decomposition and particle image velocimetry, *Med Eng Phys* **35**:898–909, 2013.
35. May P, Arrouvel C, Revol M, Servant JM, Vicaut E, Detection of hemodynamic turbulence in experimental stenosis: An *in vivo* study in the rat carotid artery, *J Vasc Res* **39**:21–29, 2002.
36. Stroka K, Espinoza AH, A biophysical view of the interplay between mechanical forces and signalling pathways during transendothelial cell migration, *FEBS J* **277**:1145–1158, 2010.
37. Himburg HA, Grzybowski DM, Hazel AL, LaMack JA, Li XM, Friedman MH, Spatial comparison between wall shear stress measures and porcine arterial endothelial permeability, *Am J Physiol Heart Circ Physiol* **286**:1916–1922, 2004.
38. Gallo D, Steinman D, Bijari PB, Morbiducci U, Helical flow in carotid bifurcation as surrogate marker of exposure to disturbed shear, *J Biomech* **45**:2398–2404, 2012.